Mapping Molecular Orbital Symmetry on High-Order Harmonic Generation Spectrum Using Two-Color Laser Fields

Hiromichi Niikura,[1,2] Nirit Dudovich,[3] D. M. Villeneuve,[1] and P. B. Corkum[1,4]

[1]*National Research Council of Canada, 100 Sussex Drive, Ottawa, Ontario, Canada K1A0R6*
[2]*PRESTO, Japan Science and Technology Agency, Sanbancho Building, 5-Sanbancho, Chiyodaku, Tokyo, Japan, 102-0075*
[3]*Department of Physics of Complex Systems, Weizmann Institute of Science, Rehovot 76100, Israel*
[4]*Department of Physics, University of Ottawa, 150 Louis Pasteur, Ottawa, Ontario, Canada K1N 6N5*

(Received 7 June 2009; published 28 July 2010)

We have measured high-order harmonic generation spectra of D_2, N_2, and CO_2 by mixing orthogonally polarized 800 and 400 nm laser fields. The intensity of the high-harmonic spectrum is modulated as we change the relative phase of the two pulses. For randomly orientated molecules, the phase of the intensity modulation depends on the symmetry of the molecular orbitals from which the high harmonics are emitted. This allows us to identify the symmetry of any orbital that contributes to high-harmonic generation, even without aligning the molecule. Our approach can be a route to imaging dynamical changes in three-dimensional molecular orbitals on a time scale as short as a few hundred attoseconds.

DOI: 10.1103/PhysRevLett.105.053003 PACS numbers: 33.80.Rv, 42.50.Hz

A high-harmonic generation spectrum contains information on atoms or molecules, such as vibrational motion [1,2], electron motion [3], and electronic structure [4–7]. Combined with molecular alignment techniques, molecular orbital tomography was demonstrated in 2004 [4], allowing us to measure the amplitude of an electronic wave function. However, there are major impediments to using molecular alignment methods for orbital tomography. First, there is an interplay between two basic processes underlying high-harmonic generation—tunnel ionization and electron recollision [8,9]. As we rotate the molecule for orbital tomography, tunneling probability is modulated and the structure of the recolliding electron changes [10,11]. Thus, the simplicity of the recolliding electron wave packet, on which orbital tomography is based, is lost. Second, low-lying orbitals can dominate at some angles for tunnel ionization probability [12,13]. It further complicates the high-harmonic generation process [14]. Third, only a relatively small class of molecules can be well aligned. These issues prohibit us from reconstructing molecular orbital with π_g symmetry from the high-harmonic spectra.

Another route for orbital tomography has been proposed by Shafir *et al.* [15]. They control electron trajectory in the continuum by applying an orthogonally polarized laser field with a wavelength of 400 nm in addition to the fundamental field at 800 nm. This allows the atomic orbital symmetry to be clearly written in the high-harmonic spectrum.

We demonstrate how molecular orbital symmetry is probed using high-harmonic generation for D_2, N_2, and CO_2 by extending this approach. We use randomly aligned molecules, where harmonics are preferentially generated from a portion of ensembles which dominates the ionization probability. This minimizes the multiorbital effect on high-harmonic spectrum. For instance, for CO_2 the ionization probability of the π_g orbital is peaked at 45° and 135° from the molecular axis [16]. For a laser intensity of $1.9 \times 10^{14}\ \mathrm{W/cm^2}$, the probability at this angle is calculated to $1.1 \times 10^{14}/\mathrm{s}$ [13,16]. This is two or three orders larger than those of the lower-lying π_u and σ_g orbitals at the molecular angles where the ionization probability has a maximum value. Thus, the π_g orbital is most likely selected by ionization.

Figure 1 illustrates the ionization and recollision process schematically. We set the polarization axis of the 800 nm (or 400 nm) laser field to the x (or y) axis, respectively. We focus only on the angles in the plane perpendicular to the propagation direction of the driving laser pulses. This is because only the high-harmonic emission propagating along the driving laser fields can be well phase matched.

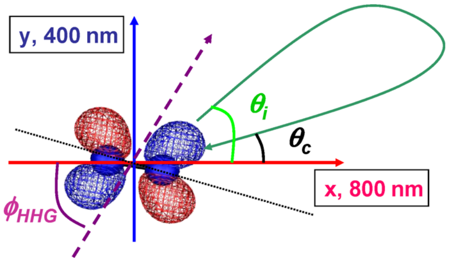

FIG. 1 (color online). A schematic picture of a molecular orbital and high-harmonic generation process. We set the polarization axis of an 800 nm (400 nm) laser pulse to the x axis (y axis), respectively. The combined fields detach an electron in the instantaneous maximum field direction at the angle of θ_i, which determines the molecular alignment. The electron returns to the parent ion with the angle of θ_c, leading to high-harmonic emission. For instance, at 13th harmonic and at a relative delay of ~0.6 fs, θ_i is ~40 and θ_c is ~0°, respectively. The resulting high-harmonic emission for the π_g orbital is polarized at $\phi_{\mathrm{HHG}} \sim 80°$. Changing the relative delay between the two laser pulses changes θ_i, θ_c, and ϕ_{HHG}. Measuring ϕ_{HHG} as a function of θ_c allows us to identify the orbital symmetry.

The physics behind our measurement can be appreciated from the strong field approximation [17]. Under this approximation, an electron is preferentially ejected to the continuum to the direction of the vector sum of the two laser polarizations at the time of ionization. We refer to this angle as the ionization angle, θ_i. For the π_g orbital in CO_2, the angular distribution of the ionization probability is peaked at 45° with a mean width of $\sim 5°$ [10]. It restricts those molecules which are responsible for high-harmonic generation to lie within the narrow cone centered along $\theta_i \pm 45°$. After ionization, the electron is accelerated by the laser fields then recollides with the molecular ion at a certain angle, referred as to the recollision angle, θ_c, leading to high-harmonic generation. The high-harmonic emission is polarized with the angle of $\phi_{\rm HHG}$. The polarization depends on both θ_c and the symmetry of the bound state wave function which recombines with the continuum electron wave packet. Thus, measurement of the relationship between $\phi_{\rm HHG}$ as a function of θ_c determines the symmetry of the bound state wave function. All angles are defined in the laboratory frame.

Instead of controlling molecular alignment, we change the phase delay between the two laser pulses, thereby changing the time-dependent field direction of the combined two-color laser fields. Changing the phase delay controls both θ_c and θ_i. This approach has advantages over the previous molecular alignment approach [16]. First, the structure of the continuum electron wave packet is less dependent of the molecular alignment angle. Second, the ionized wave packet has a definite sign relative to the bound electron wave function. These features permit us to measure the relationship between $\phi_{\rm HHG}$ and θ_c more accurately for a π_g orbital than the alignment approach, especially when θ_c is parallel to the molecular axis. Next, selecting the orientation with tunnel ionization allows us to probe molecules that cannot be easily aligned.

We measure the high-harmonic generation spectrum as a function of the relative phase delay between the two fields. Then at each delay, we obtain $\phi_{\rm HHG}$ through the high-harmonic spectrum in the laboratory frame. Because of symmetry in the combined electric fields, both even and odd harmonics appear in the spectrum. The intensity of the odd (even) harmonics is proportional to the component parallel to the polarization direction of the 800 nm (400 nm) driving laser field [15]. Then the $\phi_{\rm HHG}$ is given by

$$\phi_{\rm HHG} = \arctan(\sqrt{I_{2\omega}/I_{\omega}}), \tag{1}$$

where $I_{2\omega}$ and I_{ω} are the intensities of the adjacent even and odd harmonic orders, respectively. In order to obtain $\phi_{\rm HHG}$ as a function of θ_c for each molecule, we use D_2 as a reference. If a molecule ionizes from an almost spherical orbital like D_2, then $\phi_{\rm HHG}$ is $\sim\theta_c$. Since θ_c is a characteristic of the continuum electron and not the unaligned molecule, θ_c does not change for different molecules for the same phase delay and the same laser intensities. Then we compare $\phi_{\rm HHG}$ for D_2 with N_2 and CO_2 at given delay and harmonic number to identify the symmetry.

To produce the 400 nm laser pulse, we pass an 800 nm, 1 kHz, 35 fs, laser pulse generated from a Ti:sapphire laser system (KM Labs) through a 300 μm thick BBO crystal. We compensate the group delay between the two laser pulses with a 0.65 mm thick calcite plate. Rotating the calcite plate accumulates an extra optical path, which delays one of the laser pulses with an accuracy of <50 as. We focus the collinear laser beams into a pulsed gas jet using a 50 cm focal length mirror. The generated high-harmonic emission is spectrally dispersed by an aberration-corrected concave grating and imaged onto a microchannel plate and recorded by a CCD camera. We integrate the images over the spatial dimension to obtain the high-harmonic spectrum. We estimate the 800 and 400 nm laser intensity to be $\sim 1.1 \times 10^{14}$ W/cm^2 and $\sim 0.8 \times 10^{14}$ W/cm^2, respectively, by utilizing the cutoff photon energy.

Figure 2 shows the high-harmonic spectra of (a) D_2 and (b) CO_2 as a function of the two-color delay. We record the spectra for N_2 as well (see supplementary material [18]). Zero time delay in Fig. 2 is arbitrarily chosen. We do not need to know zero time delay accurately to identify the symmetry of a molecular orbital. As previously reported [15,19–22], even harmonics are observed as well as the odd harmonics. The spectral intensity of each harmonics is modulated with the period of $\sim$0.67 fs—half of the optical period of the 400 nm light. This is due to the fact that the same magnitude of the laser field is repeated at every half optical period of the 400 nm laser pulse.

For D_2, the peak of the high-harmonic emission is centered at the delay of $\sim$0.33 fs (and $\sim$1.00 fs) at the lowest harmonic number. The peak shifts first to smaller and then to larger phases as the harmonic number increases. The even harmonics becomes weaker for the higher harmonics. In contrast, for CO_2 we observe a very different behavior in the harmonic intensity, especially, at the low harmonics.

The time shift between two adjacent harmonics includes information on the polarization angle. Harmonics have their origin in the interference between the recolliding electron and the molecular orbital (Fig. 1). The polarization of the emitted light arises from this interference. In Fig. 3, we plot the polarization angle, $\phi_{\rm HHG}$, of the harmonics for (a) D_2, (b) N_2, and (c) CO_2 as a function of the delay and the harmonic number. In order to obtain $\phi_{\rm HHG}$, we use Eq. (1) and choose the harmonic pair of 13th + $2n$ and 14th + $2n$, where n is 0–4, respectively. We interpolate the data value along the harmonic number. The difference between D_2 (and N_2) with σ_g symmetry and CO_2 with π_g symmetry is clearly seen. At a delay of $\sim$0.30 fs and at harmonic $\sim$13, $\phi_{\rm HHG}$ is $\sim 45°$ for D_2 while $\phi_{\rm HHG}$ is $\sim 0°$ for CO_2. On the other hand, at the delay of $\sim$0.67 fs, $\phi_{\rm HHG}$ is $\sim 0°$ for D_2, while $\phi_{\rm HHG}$ for CO_2 is $\sim 90°$.

In Fig. 3(d), we plot the result of a classical electron trajectory calculation for θ_c under the two-color laser fields. We use strong field approximation and assume a

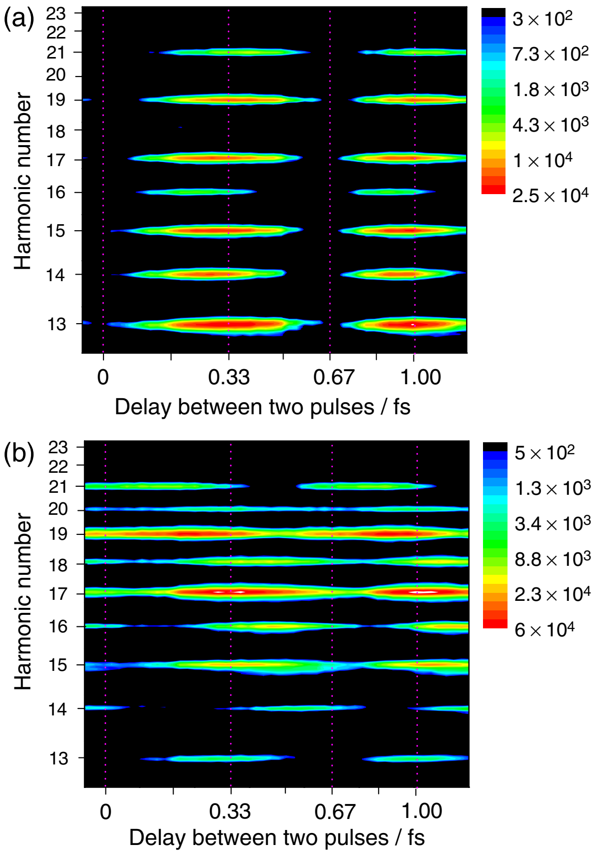

FIG. 2 (color online). High harmonic generation spectra of (a) D_2 and (b) CO_2 as a function of the phase delay between the two laser pulses. The color code represents the signal intensity.

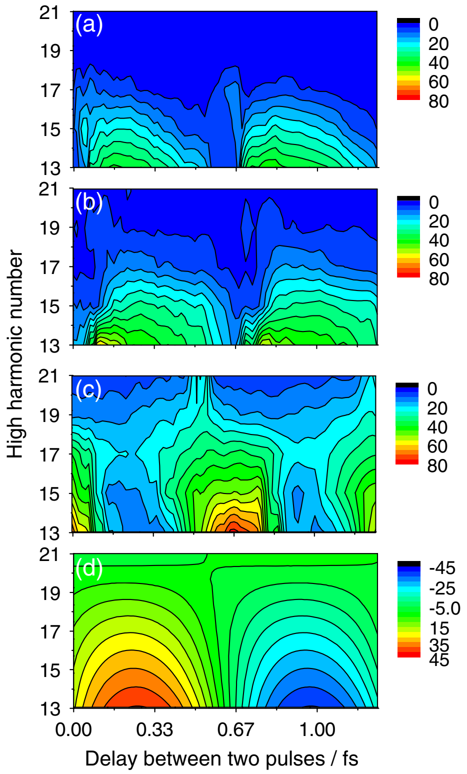

FIG. 3 (color online). Polarization angle, ϕ_{HHG}, as function of the delay and the harmonic number for (a) D_2, (b) N_2, and (c) CO_2, respectively. The angle is represented by the color coding. In (d), we plot the calculated θ_c for a spherically symmetric orbital.

totally spherical cross section. Figure 3(a) is comparable to Fig. 3(d) except for the sign of the angle which cannot be distinguished experimentally. This confirms that θ_c can be controlled by changing the phase delay, and that ϕ_{HHG} for D_2 is a measure of θ_c. While the absolute value of θ_c depends on the intensity ratio between the 800 nm and the 400 nm laser pulses, the overall structure of the distribution remains the same.

The orbital symmetry dependence of the high-harmonic polarization, that is immediately obvious in Fig. 3, is shown differently in Fig. 3. The square data points represent ϕ_{HHG} for (a) N_2 and (b) CO_2 versus ϕ_{HHG} for D_2, regarded as θ_c, for the ~13th harmonics. For N_2, the slope is positive while for CO_2 the slope is negative. To confirm that the slope is related to the symmetry of the molecular orbital, we simulate ϕ_{HHG} as a function of θ_c. We use the HOMO (π_g), the HOMO-1 (π_u), and the HOMO-2 (σ_g) of CO_2 calculated by the GAMESS program [23]. We calculate the magnitude of the dipole moment induced along the 800 nm (400 nm) polarization axis as a function of θ_c for the harmonic number at 13th and 14th, respectively, and then obtain ϕ_{HHG}. We average ϕ_{HHG} over the angular distribution of the molecular axis weighted by the ionization probability [10]. The details of the calculation are described in the supplementary material [18].

The dashed line in Fig. 4(a) represents ϕ_{HHG} as a function of θ_c when the orbital is totally spherical. In this case, ϕ_{HHG} is proportional to θ_c. The observed data points for N_2 are slightly larger than the dotted line at a given θ_c. For N_2, the tunnel ionization probability of the $2p\ \sigma_g$ orbital has an elliptical distribution along the molecular axis [14] and the orbital is elongated along the molecular axis. These facts result in the slightly large ϕ_{HHG} at a given θ_c.

In Fig. 4(b), we plot the calculated ϕ_{HHG} versus θ_c for the π_g orbital as a solid line and for the π_u orbital as a dashed line. The calculated line for the π_g has the same tendency as the observed data points, which is clearly different from the π_u. For the σ_g case, the slope of ϕ_{HHG} versus θ_c is positive as is the case of N_2's σ_g state. It is consistent that because the π_g orbital has the most loosely bound state for CO_2, as one might expect for unaligned molecules, the π_g orbital contributes predominantly to the high-harmonic generation from CO_2 at this laser intensity.

We have plotted ϕ_{HHG} as a function of θ_c in a laboratory frame. This requires minimum assumptions yet gives a clear identification of the molecular orbital symmetry. For comparison with the alignment approach [16], we plot $|\phi_{\mathrm{HHG}} - \theta_c|$ versus $\theta_{c(\mathrm{MF})}$ in the online material, where $\theta_{c(\mathrm{MF})}$ is the recollision angle in the molecular

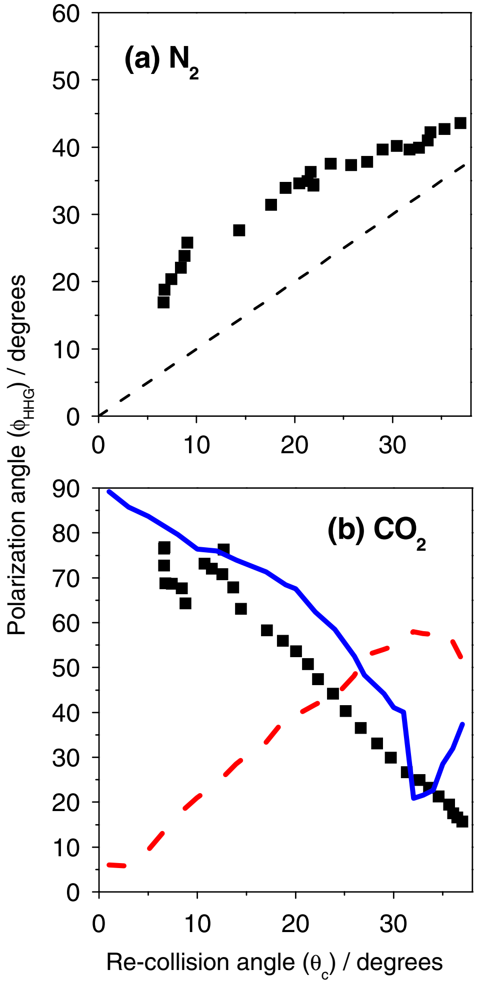

FIG. 4 (color online). The square data points show the measured ϕ_{HHG} as a function of θ_c at the ~13th harmonic for (a) N_2, (b) CO_2. The dotted line in (a) is a plot of the calculated result using a spherically symmetric molecular orbital. The solid and dashed lines in (b) are the plots of the calculated ϕ_{HHG} for the π_g and the π_u orbital of CO_2, respectively.

frame. In our results, it is possible to have a perpendicular polarization component when the electron recollides with the π_g orbital parallel to the molecular axis. This is due to the fact that the continuum carries the phase of the bound state. On the other hand, the alignment approach results in $|\phi_{\mathrm{HHG}} - \theta_c| \sim 0$ at $\theta_{c(\mathrm{MF})} \sim 0$ in the molecular frame, i.e., for the molecular axis aligned parallel to the field, by symmetry the emission must be polarized parallel to the laser field.

In summary, we have identified the orbital symmetry of the π_g orbital using high-harmonic spectroscopy, which was revealed despite the complexities and uncertainties. Our results lay out a general path to tomography of complex orbitals. We have shown that two-color fields will replace alignment in the role of obtaining multiple projections of an orbital. Combining the two-color fields, alignment will gain a new role—to select the orbital of interest.

Our approach can be extended to dynamical measurements. If, for example, a nonadiabatic process occurs at the time of tunnel ionization, then the molecular orbital may change its spatial distribution dynamically, which leads to dynamical changes in ϕ_{HHG}. Because high-harmonic order can be related to the recollision time [3], dynamical changes in the molecular orbital can be mapped onto a two-dimensional figure like Fig. 3. In Fig. 3, the ϕ_{HHG} peak appears at a delay ~0.30 fs for the σ_g orbital, while the ϕ_{HHG} peak appears at a delay ~0.67 fs for the π_g orbital. If the molecular symmetry changes from σ_g to π_g, then the changes can be traced on the map.

For our experimental conditions, the σ_g and π_u orbitals cannot be distinguished because the θ_c range is limited from 0° to ~45°. If we control the electron trajectory using a longer laser wavelength, for instance, combining 800 with 1600 nm laser pulses, we can extend the angles θ_c to ~90° . In addition, a longer laser wavelength can extend the cutoff harmonics, permitting us to measure three-dimensional molecular structure for any orbital symmetry and view dynamical changes with attosecond time resolution.

It is our pleasant duty to acknowledge extensive advice and assistance from Dr. A. Naumov. We acknowledge funding from JST and NSERC.

[1] S. Baker *et al.*, Phys. Rev. Lett. **101**, 053901 (2008).
[2] W. Li *et al.*, Science **322**, 1207 (2008).
[3] H. Niikura, D. M. Villeneuve, and P. B. Corkum, Phys. Rev. Lett. **94**, 083003 (2005).
[4] J. Itatani *et al.*, Nature (London) **432**, 867 (2004).
[5] H. J. Wrner *et al.*, Phys. Rev. Lett. **102**, 103901 (2009).
[6] T. Morishita, A. T. Le, Z. Chen, and C. D. Lin, Phys. Rev. Lett. **100**, 013903 (2008).
[7] M. Kitzler *et al.*, New J. Phys. **10**, 025029 (2008).
[8] P. Corkum, Phys. Rev. Lett. **71**, 1994 (1993).
[9] F. Krausz and M. Ivanov, Rev. Mod. Phys. **81**, 163 (2009).
[10] D. Pavicic *et al.*, Phys. Rev. Lett. **98**, 243001 (2007).
[11] C. D. Lin, X. M. Tong, and Z. X. Zhao, J. Mod. Opt. **53**, 21 (2006).
[12] O. Smirnova *et al.*, Phys. Rev. Lett. **102**, 063601 (2009).
[13] O. Smirnova *et al.*, Nature (London) **460**, 972 (2009).
[14] Y. Mairesse *et al.*, New J. Phys. **10**, 025015 (2008).
[15] D. Shafir *et al.*, Nature Phys. **5**, 412 (2009).
[16] J. Levesque *et al.*, Phys. Rev. Lett. **99**, 243001 (2007).
[17] T. Zuo, A. D. Bandrauk, M. Ivanov and P. B. Corkum, Phys. Rev. A **51**, 3991 (1995).
[18] See supplementary material at http://link.aps.org/supplemental/10.1103/PhysRevLett.105.053003 for the detailed description of the analysis.
[19] N. Dudovich *et al.*, Nature Phys. **2**, 781 (2006).
[20] T. T. Liu, T. Kanai, T. Sekikawa, and S. Watanabe, Phys. Rev. A **73**, 063823 (2006).
[21] I. J. Kim *et al.*, Phys. Rev. Lett. **94**, 243901 (2005).
[22] S. Gilbertson *et al.*, Appl. Phys. Lett. **92**, 071109 (2008).
[23] M. W. Schmidt *et al.*, J. Comput. Chem. **14**, 1347 (1993).